ACCELERATOR PHYSICS ISSUES IN LARGE PROTON STORAGE RINGS

S. Peggs
SSC Central Design Group*
LBL, 1 Cyclotron Road
Berkeley California 94720, USA

Summary

A review of some accelerator physics issues which have arisen during the design of the Superconducting Super Collider (SSC) is broken down into the following topics: Primary Constraints, Magnet Style and Orientation, Cell Parameter Optimisation, Interaction Region Optics, Beam-Beam Effects, Dipole Field Errors, Tracking Tools, and Global and Local Correction Schemes.

Introduction

The first two high energy proton accelerators to be brought into storage ring operation, the ISR and the SPS, were built using conventional iron dominated magnets. In order to reduce the power consumption of the magnets, and in order to achieve fields above the saturation limit of iron, the recently commissioned Tevatron storage ring was constructed using superconducting magnets, in which the field profile is dominated by the placement of the conductors. The financial advantage of using conductor dominated magnets increases at higher energies, so that all of the next generation of proton storage rings use superconducting magnets, whether they are under design (LHC, SSC) or construction (HERA, UNK). Another significant trend is that the number of circulating bunches which must be stored in order to achieve interesting event rates increases dramatically (~17,000 in the SSC) as energies rise and rings get longer.

A "large proton" storage ring is defined for the purposes of this discussion by the assumptions that superconducting magnets are used, and that there are very many bunches per beam. Both of these assumptions have fundamental consequences. For example, the magnetic field quality is lower in conductor dominated magnets than in iron dominated magnets, while the capital cost per meter of magnet is higher. A major design problem in the accelerator physics of high energy proton rings is therefore to determine the minimum magnet bore which gives acceptable field quality for satisfactory operation, since this has a significant impact on the overall cost of a machine. The decreased field quality also places increased demands on the lattice correction elements which are to be included, and on the correction schemes which are to be used.

The discussion which follows concentrates on selected issues which have arisen at the Central Design Group (CDG), and elsewhere, during the design of the SSC. For this reason many references are made to the Conceptual Design Report of the SSC[1], and to CDG reports. However, while parameters specific to the SSC are sometimes quoted, the important accelerator physics issues are discussed in as general a fashion as is possible. Collective effects are not discussed (except for the crucial beam-beam effect) and a comparison of proton-proton and proton-antiproton configurations[2] is avoided, in order to retain pedagogical clarity within the space available.

Primary Constraints

Suppose that the design goal of a proton storage ring is to reach a given luminosity at a given storage energy, and with a given normalised emittance. The luminosity for head on collisions at a single interaction point (IP) is

$$L = N_B^2 / S_B \cdot c / 4\pi\sigma^{*2} \qquad (1)$$

where c is the speed of light, σ^* is the rms transverse beam size (assumed equal in both dimensions), N_B is the bunch population, and S_B is the longitudinal spacing between bunches in one beam. It is common for S_B to be twice the arc length between successive symmetrically placed interaction regions (IRs) in conventional storage rings, so that there are half as many bunches as interaction points. However, in large storage rings the bunch spacing S_B must be reduced as far as possible, in order to make large luminosities with reasonable single beam populations N_B which will not, for example, violate beam-beam dynamical limits.

*Operated by the Universities Research Association for the U.S. Department of Energy.

Another reason to reduce S_B at fixed luminosity is in order to reduce <n>, the average number of events per crossing, to a tolerable level for the experiments. Some experiments may only be able to interpret one event per interaction. Figure 1 plots the relationship

$$\langle n \rangle = L S_B \Sigma_{inel} / c \qquad (2)$$

for typical SSC parameters, where $L = 10^{33}$ cm^{-2} sec^{-1} and the total proton-proton inelastic cross section $\Sigma_{inel} = 90$ millibarns. Also displayed is the efficiency of producing single event collisions, L_1 / L. The nominal spacing in the SSC is $S_B = 4.8$ meters.

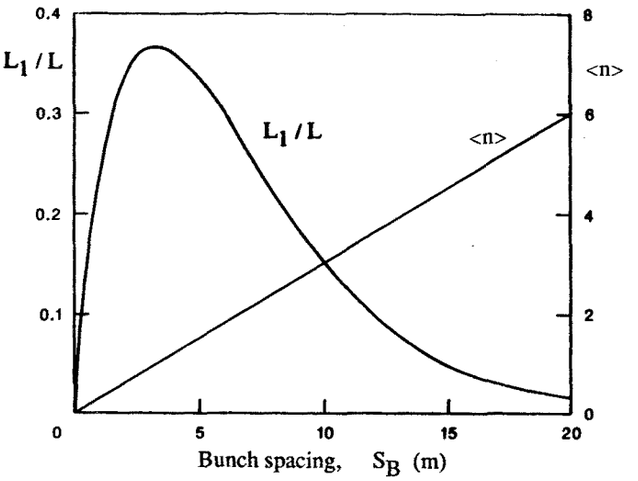

Figure 1 The average number of interactions per crossing, <n>, and the single event efficiency, L_1/L, versus bunch spacing, S_B (m)

As the bunch spacing is decreased at fixed luminosity the total beam current $I \sim N_B/S_B$ increases, since $L \sim I^2 S_B$. This has unfortunate consequences for proton storage rings where synchrotron radiation has begun to be significant, since the total radiated power per ring is

$$P = Z_0 / 3 \cdot e^2 c^2 \gamma^4 / C\rho \cdot N_T \qquad (3)$$

where Z_0 is the impedance of free space, e is the electronic charge, γ is the usual relativistic factor, C is the ring circumference, ρ is the bending radius, and N_T is the total population in one beam. This heat load (about 9 kilowatts for the SSC) is much less than electron storage ring loads, but must be removed by the refrigeration system cooling the vacuum pipe, with significant cost implications. Another limit to short bunch spacing is the ability of the experiments to reset their electronics in the time available, τ_{rep}, between bunch crossings. Figure 2 illustrates these relationships using SSC parameters.

Short bunch spacing means that there will typically be tens of locations in an interaction region, separated longitudinally by $S_B/2$, where bunches pass by each other. This mandates the introduction of a crossing angle at the principal collision point, since the experimenters want collisions at only one place. Worse, without a crossing angle the cumulative beam-beam interaction effects are usually intolerable, since the tune shift at each of the n_c head on interactions in a single IR is

$$\Delta\nu_{HO} = \xi \equiv -N_B r_p / 4\pi\varepsilon \qquad (4)$$

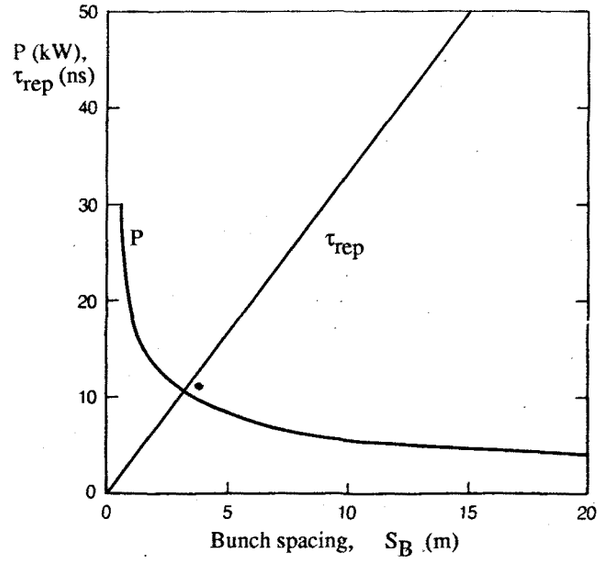

Figure 2 Dependence of the SSC synchrotron radiation power, P, and the detector repetition time, τ_{rep}, on the bunch spacing, S_B

where ξ is the beam-beam tune shift parameter, r_p is the classical proton radius, and ε is the invariant emittance.

When the crossing angle α at an IP with a beta function of β^* is large compared to σ^*/β^*, the angular size of the beam, then in addition to a tune shift given by (4) due to the single remaining (almost) head on collision, there is also a total long range tune shift which is well approximated[3,4] by

$$\Delta\nu_{LR} = n_c \, \xi \cdot \frac{2}{[\alpha / (\sigma^*/\beta^*)]^2} \qquad (5)$$

The head on tune shift is proportional to the bunch population, $\Delta\nu_{HO} \sim N_B$, while the long range shift depends on the total population, $\Delta\nu_{LR} \sim N_T$, so that varying the bunch separation S_B trades one off against the other. This is illustrated in figure 3 using SSC parameters.

The crossing angle can cause a significant loss of luminosity, since if α is large compared to σ^*/σ_s, the aspect ratio of the beam, the longitudinal tails of the bunches will not collide. The ratio of the true luminosity to the head on luminosity is

$$L / L_0 = [\, 1 + (\alpha \, \sigma_s / 2\sigma^*)^2 \,]^{-1/2} \qquad (6)$$

Attempts to increase the true luminosity by continuously reducing β^* (and σ^*) eventually run into a conflict between the need for α to be large to control the long range tune shift, and the need for α to be small in order to achieve a reasonable fraction of the available head on luminosity. Angles much smaller than the profile angle are also preferred for beam-beam reasons, because odd resonances and satellite resonances are then partially suppressed[5,6].

In addition to constraints on physical parameters, there are also primary constraints on operational aspects of accelerator control, measurement, and correction. In the most fortunate electron storage rings the entire cycle of reinjection and transition to storage conditions may take as little as a few minutes, with injection repetition rates of tens of Hertz. This permits the operator to feel confident in tuning injection, for example, by turning knobs in an almost ad hoc manner in real time, since in the worst case only a negligible amount of "up-time" will be lost. By contrast, the time to refill a large superconducting ring is of order one hour, partly because of the need to avoid eddy current heating in the cold vacuum pipe during the ramp to top energy, and partly because injection itself is a slow process. A superconducting ring is especially susceptible to catastrophic beam loss during ad hoc tuning, since the loss of only a small portion of the beam into the walls will cause one or more magnets to quench and go normal (or cause a beam abort).

As the size and response time of large proton storage rings

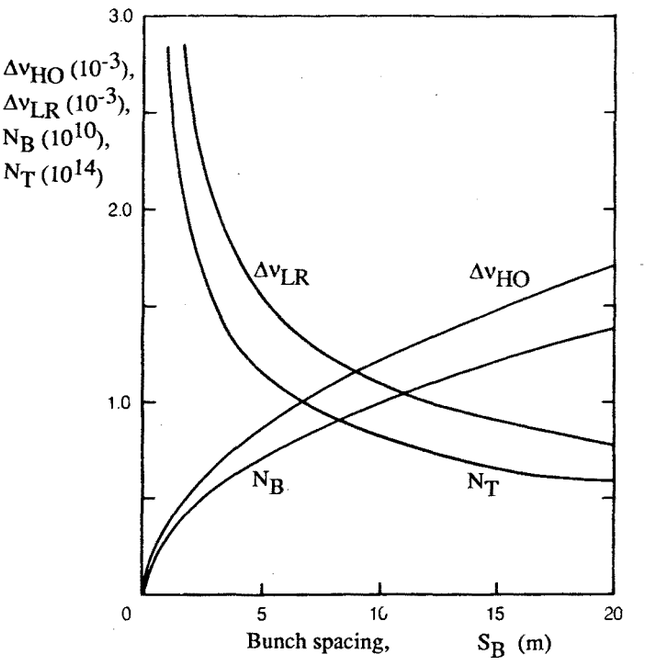

Figure 3 Dependence of the SSC head on and long range beam beam tune shifts $\Delta\nu_{HO}$ and $\Delta\nu_{LR}$, the bunch population N_B, and the total beam population N_T, on the bunch spacing S_B.

increase, the need for intelligent accelerator control - better algorithms, better diagnostics, better controls - becomes more heavily emphasised. To continue the example, it must be possible to tune up injection in a small number of rational correction iterations. Unfortunately, the need for more diagnostics and control hardware is somewhat in conflict with the superconducting nature of a high energy ring, through the increased costs and difficulties of enclosing hardware in cryostats, and through the need to avoid increased heat loads.

Magnet Style and Orientation

If the colliding beams are protons and antiprotons, then they may travel through the same beam pipe in a single ring of magnets - although their closed orbits need to be separated almost everywhere, and the magnet bore must be larger[2]. It is assumed here that both beams consist of protons, in which case two rings of magnets are required, with three general classes of magnet construction style.

"One-in-one" magnets, with the magnets of each ring in separate cryostats, have the virtue that the rings may be placed side-by-side, or one on top of the other. The magnetic errors of each ring are independent, as are the misalignment errors, and the beam separation may be increased at will, above the minimum value of twice the cryostat wall radius. One ring may be operated independently of the other, perhaps even at a different energy.

"Two-in-one magnetically uncoupled" magnets, with both rings in a single cryostat, form a more complicated package. The two rings share misalignment errors and share some magnetic errors, but the total heat leak per meter is lower than for one-in-one magnets, due to the decreased total surface area. The rings may be separated vertically or horizontally, but the beam separation has a maximum value which is smaller than the minimum value in one-in-one magnets.

"Two-in-one magnetically coupled" magnets, with both magnets sharing the same flux return yoke, reach slightly higher fields more easily. However, magnetic field and misalignment errors are coupled between the two rings, leading to operational complications. Their use naturally leads to a horizontal orientation of the two rings, so that the flux flowing up through one vacuum pipe flows down through the other.

A vertical separation of the two rings has the advantage of simpler beam injection and abort, less magnetic coupling in a

two-in-one magnet, easier magnet installation and change procedures for one-in-one magnets, and more efficient use of tunnel floor space. Horizontal separation has the slight advantage of making dispersion control easier at the collision points, but makes it difficult to match the two ring circumferences when the IRs are "clustered" with an even number of IRs in each cluster.

None of these arguments conclusively favor one or other magnet construction style or separation orientation. In the case of the SSC it was decided that a one-in-one design is preferable from an operational point of view for the majority of the circumference, even at a modest premium in capital cost, and that vertical ring separation is preferred[7]. Figure 4 shows a prototype SSC dipole in its cryostat.

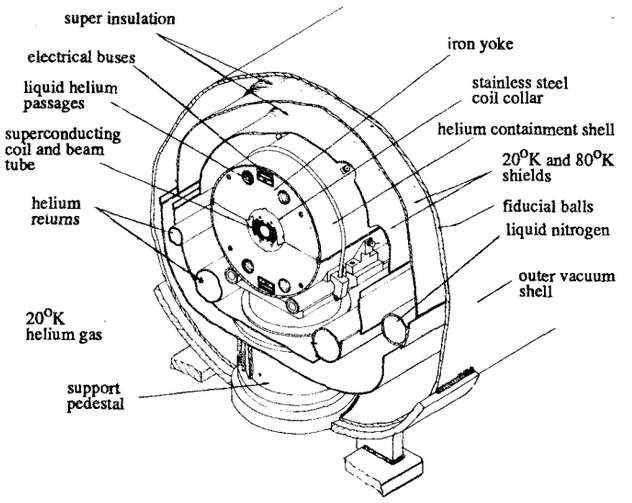

Figure 4 Perspective drawing of the 6.6 Tesla SSC dipole magnet

Optimisation of Cell Length, Cell Phase Advance, and Dipole Bore

The cost of the regular FODO cell magnets dominates the total magnet cost in a high energy proton storage ring[8]. One algorithm to minimise this cost is to first parameterise the cost per cell, and the performance of a collider made of such cells, in terms of the cell half-length L_h, the cell phase advance ϕ, and the diameter of the magnet bore, d . If the tools to fully analyse a particular configuration are available, then two dimensional surfaces of constant performance, and of constant cost, may be explored in the three dimensional (L_h, ϕ, d) space. A cost minimising solution is found on the surface of minimum acceptable performance.

The process of determining the linear and dynamic apertures, which quantify the storage ring performance in a particular configuration, is complex and computationally intensive, as discussed further below. Qualitatively, the physical effects which enter into the optimisation are well illustrated by considering a FODO cell full of dipoles, with a thin chromatic sextupole next to each thin quadrupole. The quadrupole strength q, the minimum and maximum betas, and the minimum and maximum dispersions η, are given, with $s = \sin(\phi/2)$, by

$$q = 1/f = 2s/L_h \qquad (7)$$

$$\begin{aligned} \beta_{min} &= L_h/s \,.\, [(1-s)/(1+s)]^{1/2} \\ \beta_{max} &= L_h/s \,.\, [(1+s)/(1-s)]^{1/2} \end{aligned} \qquad (8)$$

$$\begin{aligned} \eta_{min} &= L_h^2/\rho \,.\, (2-s)/2s^2 \\ \eta_{max} &= L_h^2/\rho \,.\, (2+s)/2s^2 \end{aligned} \qquad (9)$$

First consider holding L_h constant, and varying d and ϕ. There is a critical radius in the bore of a dipole, inside which the magnetic field varies from the nominal by less than, say, three parts in ten thousand. As a rule of thumb, which will be justified below, this "good field region" is a constant fraction of the bore radius, say about two thirds. Beyond this radius the field deteriorates very rapidly if, as usual, random high order multipole errors dominate. A particle is lost, in a naive model, if it ever once strays outside the good field region, defining a dynamic aperture which is easily matched to operational requirements by adjusting the bore diameter. The aperture required for an on energy particle of given emittance may also be modifed by altering β_{max}, but equation (8) shows that its variation with ϕ is very weak, at least over the range of interest between 60 and 90 degrees. On the other hand, equation (9) shows that the maximum dispersion is almost halved in going from 60 to 90 degrees, explaining the observation from SSC tracking that off momentum particles prefer a high phase advance per cell.

Now consider varying L_h, the cell half length. Both β_{max} and η_{max} decrease with L_h, making short cells look attractive. So far, however, it has been implicitly assumed that the dynamic aperture due to the chromatic sextupoles alone is much larger than the bore. In fact the chromatic dynamic aperture decreases dramatically with the cell length, since the sextupole strengths are proportional to q/η, and therefore to L_h^{-3}, according to (7) and (9). This is one effect limiting the cell length from below. Shorter cells also lead to a larger total number of elements. The length of the quadrupole increases in proportion to its focal strength, and in inverse proportion to the cell length, since there is a maximum attainable quadrupole gradient. This causes the machine circumference to increase with decreasing cell length. These last two effects have cost implications, and so also limit the cell length from below. (It is interesting to note that the maximum regular cell dispersion, 3.9 meters in the SSC, is roughly constant over most electron and proton accelerators.)

Interaction Region Optics

Turning from the most common optical unit to the most specialised, the interaction region optics must maximise the luminosity by focusing the beams down to as small a size as possible. One method of matching $\beta^* = 1.0$ meter collision beta functions into the regular cell values is shown in figure 5, where regular cells with $L_h = 100$ meters and $\phi = 60$ degrees start at the fifth quadrupole[9]. In this example there is an experimental drift meters length $L^* = 20$ meters before the front face of the first quadrupole in the IR triplet, which has a total length of about 50 meters.

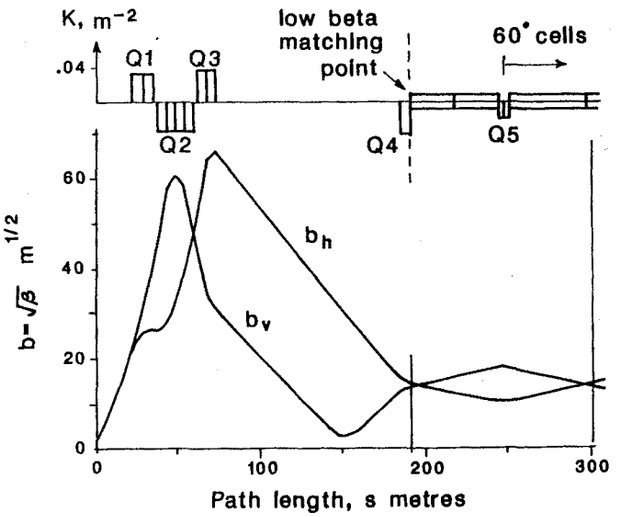

Figure 5 One scheme to match low beta insertion optics, with β^*=1.0 meter, to the optics of 60 degree regular cells.

If the quadrupole field strength is K, (with a maximum allowed value of about 0.04 meters^{-2} for SSC IR quadrupoles), then in general the beta functions obey the differential equation

$$b'' + K b - b^{-3} = 0 \qquad (10)$$

where

$$b = \beta^{1/2} \qquad (11)$$

and K has a different sign in different planes. The primes refer to

differentiation with respect to s, the longitudinal coordinate. In the experimental drift K=0, so that if s=0 and b'=0 at the collision point, equation (10) is solved to give

$$\beta(s) = \beta^* + s^2/\beta^* \qquad (12)$$

so that the β value entering the triplet, which sets the scale for the values in the triplet, is inversely proportional to the collision beta. If β^* is reduced by a factor of four, for example, and the vertical scale in the figure is contracted by a factor of two, the new and the old beta curves would be virtually indistinguishable out to the fourth quadrupole, at about 190 meters. The betas beyond this point would not match into their regular cell values, but the four rematching conditions may be met by very slightly adjusting the three triplet quadrupole strengths, and making a more significant change in the strength of the fourth quadrupole.

The matching process can be understood as follows. Equations (10) and (12) illustrate that the slope b' is constant, to a good approximation, when K=0 and β is high enough that the betatron phase advances slowly. This explains why the b_h and b_v curves just after the triplet are straight lines - which have been focused by the triplet to be roughly parallel. The horizontal beta goes through a minimum at s≈150 meters, but the slope b'_h quickly approaches its new asymptotic value, equal and opposite to its old asymptote, so that $b_h' \approx -b_v'$ at the entrance to the fourth quadrupole. Equation (10) is readily integrated across a thin quadrupole, of focal strength q, to give

$$b_{out} = b_{in}, \qquad b'_{out} = b'_{in} + q\, b_{in} \qquad (13)$$

This shows that the horizontal and vertical slope increments in the fourth quadrupole are roughly equal and opposite, since $b_h \approx b_v$ there, so it remains true that $b_h' \approx -b_v'$ even after exiting. These two approximate equalities are made exact, and become matching conditions, if the distance from the exit face of the fourth quad to the center of the fifth quad is one quarter of a cell length, since then the exit face is in the middle of a half cell.

It is also necessary to match the horizontal dispersion from its value of zero at the collision point to its regular cell value. This is readily done for any cell phase advance using a 'missing dipole' scheme. For example, if the first and third of the 60 degree cells following quadrupole 5 contain no dipoles at all, while the second cell has the normal dipole structure, then integration of the differential equation describing dispersion propagation

$$\eta'' + K\eta = G \qquad (14)$$

shows that the dispersion entering the fourth cell is perfectly matched. Here G is the dipole strength, the inverse bending radius.

There also may be the problem of separating the beams into two vertically displaced rings in the main arcs, without introducing vertical dispersion. One proposed way of doing this in the SSC is shown in figure 6 (with different optics than those shown in figure 5), where two beam separation "steps" of 0.35 meters are made by placing equal and opposite vertical bends at either end of a drift[10]. If the vertical dispersion and its slope are zero at the beginning of the first step, then integration of (14) (with an appropriate sign convention) shows that at the end of the step

$$\eta'_{1\,out} = 0, \qquad \eta_{1\,out} = -\Delta v_1 \qquad (15)$$

where Δv_1 is the vertical displacement of one beam. Equation (14) also shows that in the absence of vertical dipoles the dispersion propagates like a free particle, so that passage through the "QV" section in the figure, with a phase advance of 180 degrees (and β'=0 at the entrance and exit) gives

$$\eta'_{2\,in} = -\eta'_{1\,out}, \qquad \eta_{2\,in} = -\eta_{1\,out} \qquad (16)$$

Finally, integration over the second step gives

$$\eta'_{2\,out} = \eta'_{2\,in}, \qquad \eta_{2\,out} = \eta_{2\,in} - \Delta v_2 \qquad (17)$$

Equations (15), (16), and (17) may be combined to show that there is no vertical dispersion wave in the regular cells when $\Delta v_1 = \Delta v_2$.

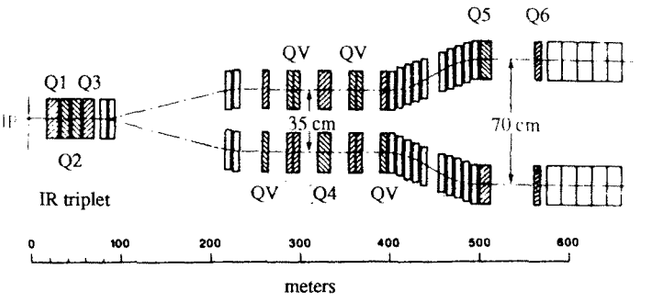

Figure 6 One proposed way of vertically separating the beams near an interaction point (IP) in the SSC. Open rectangles are vertical or horizontal dipoles; cross-hatched rectangles are quadrupoles.

Another vertical separation scheme proposed for the SSC, consistent with the geometry of figure 5, rests on the fact that the vertical dispersion caused by a step is exactly cancelled by a similar step at a place with identical beta functions 180 degrees downstream[9]. This means that the first step must be in a regular cell region - after quadrupole 4 in figure 5 - with the disadvantage of additional long range beam-beam interactions in the drift between quadrupoles three and four. The advantage of this scheme is that it makes the QV section of figure 6 unnecessary, so that the strong quadrupoles and high betas which occur there can be removed, leaving a simpler lattice with shorter interaction region optics.

The minimum useful value of β^* which can be made using optics like those described above is often limited by the maximum allowable peak value of beta, which is inversely proportional to β^* and occurs in the IR triplet[11,12,13]. For example, SSC tracking results show that, in addition to the triplet being the physical aperture stop when β^*≈0.5 meters, the peak beta of around 8 kilometers causes an extreme sensitivity to magnetic field errors, making careful multipole compensation of the IR quadrupoles necessary[14]. The triplet shown in figures 5 and 6 is already much longer than the experimental drift. If the bore of the triplet quadrupoles is increased, the maximum gradient they can make decreases in roughly inverse proportion, so that the quadrupoles must be made even longer, which in turn increases the peak beta even further.

There is no longer a compelling reason to distribute the many IRs symmetrically, since there are many more bunches than IRs in a large proton collider, and since random field errors completely break the advantageous symmetry that superperiodicity offers in storage rings with iron dominated magnets. Figure 7 shows how it is proposed to combine the SSC experimental interaction regions, and the injection and extraction regions, into two "clusters" of four 'straight' sections[15]. The bending loss in each of the eight 'straight' sections is identical, assuring closure of the lattice. The main benefits of clustered IRs are economic and social, since fewer roads are needed, and limited resources are better shared, for example. However, the chromatic properties of the lattice are also improved somewhat by arranging IRs with common β^* values in pairs, with an odd integer number of quarter wavelengths in betatron phase between adjacent interaction points[15,16]. This also leads to the systematic suppression of some beam-beam resonances[15].

Beam-Beam Effects

The angular kick due to a single round beam-beam interaction is given in general by

$$\Delta x' = -\frac{4\pi\xi}{\beta}\,\frac{2\sigma^2}{r^2}\,(1-e^{-r^2/2\sigma^2})\quad x \qquad (18)$$

$$\Delta y' = -\frac{4\pi\xi}{\beta}\,\frac{2\sigma^2}{r^2}\,(1-e^{-r^2/2\sigma^2}).\,(y+d_y) \qquad (19)$$

where

$$r^2 = x^2 + (y+d_y)^2 \qquad (20)$$

Here x and y are horizontal and vertical coordinates measuring the

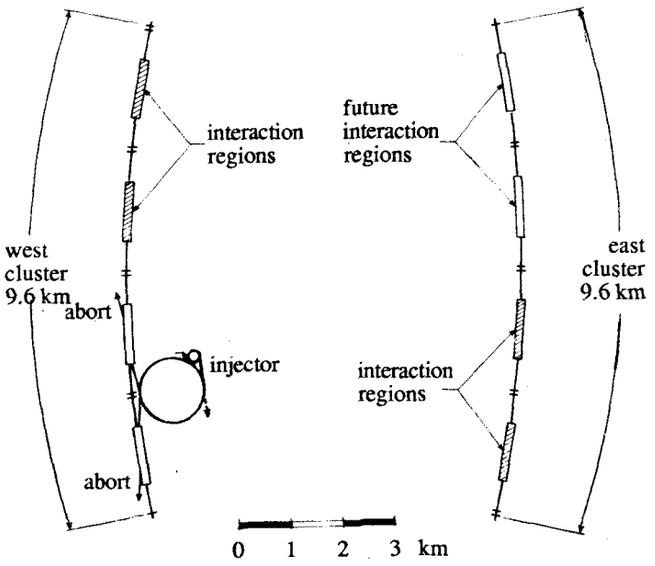

Figure 7 The proposed arrangement of SSC interaction regions, injection, and extraction straights into east and west "clusters".

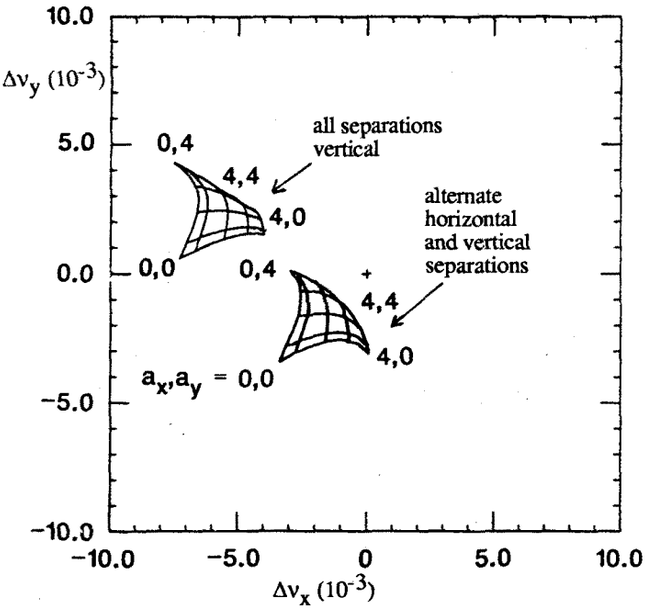

Figure 8 Total tune shifts and spreads due to head on and long range beam beam interactions in a typical SSC lattice.

displacement of a test particle from the center of its own beam, and d_y is the separation of the two beams (assumed vertical). Typical particles have displacements of order σ, so that the exponential in (18) and (19) commonly changes a great deal from turn to turn when the interactions are head on ($d_y = 0$), leading to strong nonlinear behavior. Long range ($d_y >> \sigma$) collisions are relatively linear by contrast, since the exponential essentially vanishes, leaving a smoother 1/r dependence. Head on interactions are therefore more dangerous for driving nonlinear resonances, while long range interactions are more dangerous for spreading the beam over a large area in the $\{\nu_x,\nu_y\}$ tune plane, where both beam-beam and magnetic resonances must be avoided.

Tune Shifts and Spreads

In the small amplitude limit of head on interactions a quadrupole approximation

$$\{\Delta x', \Delta y'\} \approx -\frac{4\pi\xi}{\beta}\{x, y\} \qquad (21)$$

shows that the head on tune shift is the same in both planes. In the small amplitude limit of a single long range interaction the approximation to quadrupole order

$$\{\Delta x', \Delta y'\} \approx \frac{4\pi\xi}{\beta}\frac{2}{(d_y/\sigma)^2}\{x, d_y - y\} \qquad (22)$$

also contains a dipole term which modifies the vertical closed orbit. The long range tune shifts are equal and opposite in the two planes, and are smaller than the head on tune shift by a factor which is quadratic in the beam separation (recall equations (4) and (5)).

Figure 8 shows beam-beam tune shifts and spreads in two proposed configurations of the SSC, both with β^*=0.5 meters in two IRs including 60 long range interactions, and with β^*=10.0 meters in two IRs including125 long range interactions[4]. The tune shift parameter is ξ=−8.2 10^{-4}, and the crossing angle α is 75 microradians. Figure 8a shows the tune shift for a web of amplitudes, $a_x\sigma$ and $a_y\sigma$, when the separation angle at all four IRs is in the vertical plane. Figure 8b shows how the sign difference in the quadrupole term in (22) leads to a reduction in the tune shift when the crossing plane alternates - which it is possible to do without changing the macroscopic orientation of the rings.

Beam-Beam Resonances

A model of chaotic behavior through resonance sideband overlap leads to a good quantitative understanding the marginal importance of 10th order beam-beam resonances in the SPS, where there are 6 head on collisions of strength $\xi\approx$0.004 per turn[6,17,18]. A key ingredient of the one dimensional theory is the assumption that the betatron tune is modulated by some mechanism at a low frequency ν_s, so that

$$\nu = \nu_0 + \delta\nu\cos(2\pi\nu_s t) \qquad (23)$$

where ν_0 is the unperturbed design tune, and t is the turn number. For example, a modulation amplitude of $\delta\nu \approx 0.001$ might come from energy oscillations coupled to a non-zero chromaticity, or from quadrupole power supply ripple. Tune modulation splits a (beam-beam or magnetic) resonance of order m into a family of sidebands

$$\nu(a) = \frac{p}{m} + k\frac{\nu_s}{m} \qquad (p, m, k \text{ integer}) \qquad (24)$$

where a is the betatron amplitude, and where only those sidebands within about $\delta\nu$ of the fundamental are important.

If the detuning function, $\nu(a)-\nu_0$, is known off resonance - as in figure 8, for example - then (24) may be solved to find the amplitude at the center of a given sideband when the tune spread is moved across the resonance. Particles with amplitudes less than the "resonance amplitude width" away from the central value are liable to lock on to the sideband, so that their trajectories circulate islands in phase space. If the amplitude width of neighboring sideband islands is larger than their amplitude separation, then according to the Chirikov criterion the independent island structure is destroyed, and chaos ensues[19]. This often means that the amplitude of a particle is free to wander over a range of amplitudes roughly corresponding to the range of tunes within $\delta\nu$ of the fundamental.

For example, figure 9a shows the results of a numerical simulation with a single head on collision per turn of strength ξ=0.006, with a tune ν_0=0.331, close to a sixth order resonance[20]. Only the main resonance islands are seen in the absence of tune modulation, centered on an amplitude about 2.7 times the beam size. When in figure 9b a tune modulation of depth 0.001 is turned on at a frequency of ν_s=0.005, sidebands k = +1, 0, -1 and -2 appear at increasing amplitudes. The sideband islands are partially submerged in a chaotic sea which extends from a minimum amplitude of about 2σ to beyond 6σ. This is in surprisingly good agreement with the quantitative results of the theory, plotted in figure 10, which state that chaos should become possible on sixth order resonances down to an amplitude of 2σ for

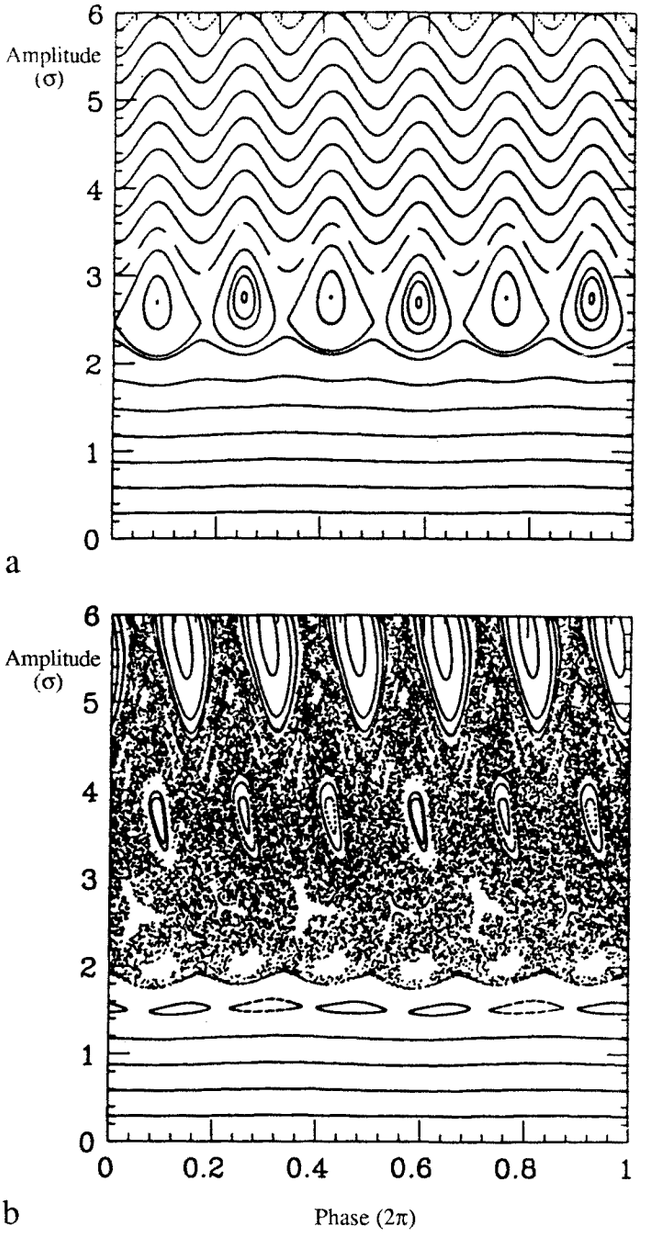

Figure 9 Simulated trajectories tracked for 2000 synchrotron periods, with a single head on beam beam interaction per turn of strength ξ=0.006, and an unshifted tune of ν_0=0.331 . (a) No tune modulation. (b) With a tune modulation amplitude $\delta\nu$=0.001 at a frequency ν_s=0.005, showing sidebands surrounded by chaos.

tune shift parameters above about 0.0063 .

Theory and simulation are also in agreement with experiment in observing that lower frequency tune modulation sources are more dangerous. (One reason that this theory is less applicable to electron storage rings than to proton rings is that the former have synchrotron tunes about an order of magnitude larger than the latter.) Theory and simulation of the coherent aspects of the long range beam beam interaction are also in good agreement, showing that coherent dipole modes of the many bunches in the two beams interactions are present at some tunes, but are not in general dangerous, at least for SSC parameters[21,22]. These agreements are pleasing, but more realistic features - such as many head on collisions per turn, incoherent long range interactions, and a second transverse dimension - must also be included in a complete analysis of the beam-beam effect. This is much easier to do in numerical simulations than in theoretical models, but theoretical insight continues to be invaluable in understanding

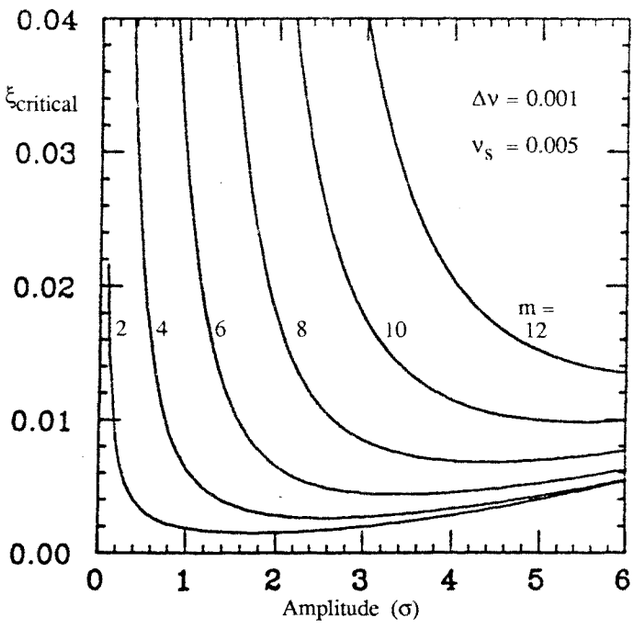

Figure 10 Critical strength $\xi_{critical}$, for a single head on beam beam collision per turn to cause chaos, by the overlap of sidebands around a resonance of order m, as a function of amplitude.

numerical results.

Dipole Field Errors

The two dimensional field in any magnet can be specified by a multipole expansion according to

$$B_y + iB_x = B_0 \sum_{n=0}^{\infty} (b_n + ia_n)(x + iy)^n \qquad (25)$$

For example, a perfect dipole would have b_0=1, or a perfect skew quadrupole would have a_1=1, with all other terms zero. This notation also lends itself naturally to a description of magnetic field errors in dipoles, which are the dominant sources of optical errors in large superconducting storage rings. The normal and skew coefficients b_n and a_n can be derived directly from Fourier analysing the voltage on a rotating coil measuring device inside a magnet. (Note that coefficients are often quoted in the "engineering" units of $10^{-4}cm^{-n}$, so that error values of order one are typical in a magnet with a bore of a few centimeters.)

Systematic Errors

Systematic contributions to even order normal multipole coefficients, b_{2n}, come from persistent current magnetisation in the superconducting wires, from saturation in the iron in the cryostat, and from systematic conductor placement errors. The strongest of the three sources is the persistent current effect, in which each superconductor filament tries to exclude magnetic flux by arranging its current density in a nonuniform distribution. Less flux can be excluded at higher fields, so that the problem is most severe at the injection energy. One way to alleviate the situation is to use the smallest possible filament diameter. Another way is to raise the injection energy and field.

The worst property of systematic errors is their ability to cause large tune shifts. The tune shift of a particle with betatron amplitude A_β and energy offset δ, in a ring made solely of regular cells, due to an error b_n, is

$$\Delta\nu_n = b_n < \beta \cos(\phi) [\eta\delta + A_\beta (\beta/\beta_{max})^{1/2} \cos(\phi)]^n > \qquad (26)$$

where two independent averages are taken, over the phase of a betatron oscillation ϕ, and over the beta and dispersion values in a regular cell. In a "smooth" approximation, where β and η take on their average cell values, this reduces to[2]

$$\Delta\nu_n = b_n\beta \sum_i C^n_{2i+1} C^{2i+2}_{i+1} 4^{-i-1} A_\beta^{2i} (\eta\delta)^{n-2i-1} \quad (27)$$

with $C^i_j \equiv i! / j!\,(i-j)!$

Table 1 shows the maximum systematic multipole errors which can be allowed in order to satisfy the SSC injection criterion that no single systematic multipole will cause a tune shift $\Delta\nu_n$ of larger than 0.005, to a particle with δ=0.001 and with A_β=0.5 centimeters.

Figure 11 shows that the computed persistent current sextupole and decapole coefficients in the proposed SSC dipole, on the increasing field side of the hysteresis loops, are in violation of the injection criterion. Distributed sextupole windings wrapped along the length of the vacuum pipe are envisaged, to correct the problem as close to its source as possible. The less critical decapole field will be corrected either with similar distributed windings, or with lumped decapoles in some of the correction packages immediately adjacent to each quadrupole.

Systematic multipole coefficient	Maximum allowed value (10^{-4} at 1 cm.)
b_2	0.0076
b_4	0.018
b_6	0.040
b_8	0.089
b_{10}	0.19

Table 1. Maximum allowable systematic multipole errors in the SSC dipoles at injection.

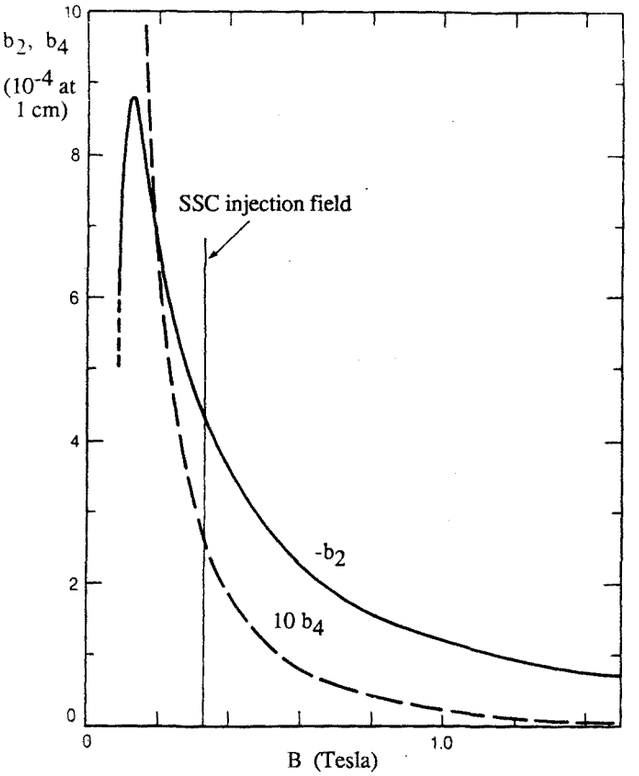

Figure 11 Calculated systematic sextupole and decapole multipole coefficients, b_2 and b_4, due to persistent currents in 5μm superconducting filaments in the SSC dipole.

Random Errors

Random contributions to the normal and skew multipole coefficients come from conductor placement errors, and from the spread in the distribution of filament sizes and critical currents. Measurements on many Tevatron, CBA, and SSC superconducting dipoles of various amplitudes have lead to an empirical scaling of the coefficients with the magnet bore, d

$$\langle a_n^2\rangle^{1/2}, \ \langle b_n^2\rangle^{1/2} \sim d^{-n-1/2} \quad (28)$$

which is also in good agreement with theoretical models of construction errors[23]. Comparison with (25) reveals the physical meaning of this scaling: except for the −1/2 term in the exponent, there is a statistically invariant fractional field error at a given fraction of the bore radius. This justifies the good field rule of thumb which was used above in the discussion of optimum cell parameters.

One way to directly correct a single random multipole error is by "sorting" the dipoles on their measured values of that coefficient. For example, the 60 dipoles in each betatron wavelength of the SSC can be arranged in the following sequence: most positive random b_2, most negative random b_2, second most positive random b_2, ... thirtieth most negative random b_2. This was found to increase the "linear aperture" (defined below) of an ensemble of five SSC lattices, each with a different set of random errors, from 5.5±1.3 millimeters to 8.9±2.0 millimeters[24]. An alternative way of correcting random sextupoles errors, proposed for the SSC, is to power the persistent current sextupole winding in a dipole from one of several alternative buses, each carrying a slightly different current, chosen according to the measured sextupole coefficient of that dipole[25]. This reduces the random sextupole component to the resolution of the buses, leaving the sorting technique available for correcting another random multipole coefficient, such as the skew sextupole.

Tracking Tools

Tracking studies have traditionally concentrated on evaluating the dynamic aperture of a lattice - the oscillation amplitude beyond which particles are lost to very large amplitudes in a given number of turns. Since injected beams are quickly damped onto the closed orbit, and unstable beams are even more rapidly aborted, a large enough dynamic aperture need only be guaranteed for of order a thousand turns. It is more important to guarantee a large enough "linear" aperture, inside which the motion is stable and sufficiently predictable for operational success. A typical definition of the on momentum linear aperture, adopted for SSC design studies, says that the tune shift may not exceed 0.005, and that a quantity called the "smear" may not exceed 10 per cent.

In linear motion the trajectory of a particle in phase space is a perfect ellipse, and the Courant-Snyder amplitude is a true invariant. When nonlinearities are present the value of the 'invariant' fluctuates from turn to turn with an rms fractional value which is the smear. The contribution of linear coupling to the smear must be removed in order for it to be a practical measure of nonlinearities in tracking studies, and the definition must be extended to two dimensions. Linear aperture measurement has nonetheless proven to be a straightforward and robust process in SSC studies, since both the smear and the tune shift rapidly converge to stable values, after only of order 200 turns. These studies show that the linear aperture depends mostly on the lower order multipoles, while the dynamic aperture depends mostly on higher order random multipoles.

Although the linearity of a fixed momentum particle is readily measured in a few hundred turns, trajectories must be tracked with energy oscillations for many synchrotron periods in order to make any statement about the potential presence of synchrobetatron sidebands, or about their possible overlap. This can easily increase the time required for a typical computer run using a conventional tracking program by two orders of magnitude, to a level which is almost prohibitive for a machine like the SSC with of order 10,000 magnets in each ring. Various attempts to avoid this slowdown are being made[26,27], or have been made[28], by summarising the motion through a large segment of a lattice, usually a single turn, in terms of a single transfer map. At the time of writing, however, these fast tracking methods are only partially successful, since they either use a limited multipole representation, or work only in one transverse dimension.

Table 2 shows the theoretically expected sensitivity of the SSC to chaos caused by random multipole errors in the dipoles. The third

Resonance order, n	$<b_{n-1}^2>^{1/2}$ (10^{-4} cm^{-n+1})	Minimum ν_s
3	2.01	$1.2 \ 10^{-1}$
4	0.35	$2.7 \ 10^{-2}$
5	0.59	$1.8 \ 10^{-2}$
6	0.059	$3.0 \ 10^{-3}$
7	0.075	$1.7 \ 10^{-3}$
8	0.016	$4.0 \ 10^{-4}$
9	0.021	$2.3 \ 10^{-4}$
10	0.003	$4.4 \ 10^{-5}$

Table 2. The estimated random normal error multipole components in the SSC dipoles, $<b_{n-1}^2>^{1/2}$, and the minimum synchrotron frequency, ν_s, to avoid chaos on an n'th order magnetic resonance.

column shows the minimum synchrotron frequency necessary to avoid the overlap of synchrobetatron sidebands for a particle with a tune modulation amplitude of 0.001, and with a 10σ betatron oscillation amplitude. The perturbation calculation used was first order in multipole strength, ignoring, for example, octupole effects caused by cross terms between sextupoles[29].

The fraction of the dynamic aperture which is linear increases significantly as sextupole and octupole errors are removed, or corrected. Studies also show that operational procedures such as closed orbit correction and the removal of coupling are important in increasing the linear aperture[30]. A tracking program used as a basis on which to test out such correction schemes naturally develops into a tailor-made operational simulation of a particular storage ring design[31]. This tendency is to be encouraged so long as the simulation does not become too slow or inflexible. Long range beam beam interactions may be the most difficult objects to self-consistently introduce into a tracking or simulation program, since they introduce a mutual interaction between the optics and closed orbits of the two rings, even if coherent effects are ignored.

Global and Local Correction Schemes

Global correction schemes must be used to remove residual linear and sextupole optical perturbations. Linear coupling is conventionally removed by tuning two skew quadrupole circuits to reduce the closest possible approach of the two eigentunes to zero, within experimental resolution[32]. This corresponds to modifying, but not totally removing, the off diagonal two by two blocks in the four by four linear matrix, R, which describes linear propagation around a single turn. An ideal lattice would also have all (non chromatic) elements of its second order T matrix zero.

The general difficulty is not in providing enough correctors, or in deciding upon orthogonal corrector locations, but rather in finding suitable diagnostics, and in finding a rapidly convergent correction algorithm. For example, a traditional method of global sextupole correction has been to measure and reduce the stop band widths of third order resonances, by moving the operating point in the tune plane to each resonance in turn. Unfortunately the tune plane movement itself modifies T, and convergence is neither rapid nor guaranteed. A similar but better method may be to kick the beam on one turn, and then to Fourier analyse the subsequent motion observed by a beam position monitor[33]. This gives the amplitude and phase of spectral lines caused by global sextupole nonlinearities, which may then be reduced.

Random walk accumulation of errors can be very serious in large storage rings with tunes of order 100, causing local fluctuations which must be removed by local correction schemes. Beta error waves and the tilting of betatron oscillation planes, for example, are only partially removed by global correction schemes. Local schemes suffer even more than global schemes from a scarcity of available diagnostics - with the exception of beta function measurement. (Beta functions at a single quadrupole are measured by noting the tune shifts caused by a small perturbation in the quadrupole strength).

One possible way to measure the local R and T matrices describing motion between two points is to adapt a technique used in "dynamic tracking". This technique combines position information from two adjacent monitors with a knowledge of the optics in between them, in order to calculate the position of the beam centroid at one of the monitors in four dimensional phase space. Dynamic tracking experiments do this in order to record phase space information turn by turn, after an initial beam excitation, prior to further analysis or plotting[34,35]. A nondestructive local "transfer function" measurement would use this technique to find the phase space location of the closed orbit at the beginning and end of the segment of interest[36]. If this is done for a set of different closed orbits by perturbing four dipole correctors outside the segment, enough redundant information can be found to determine the R and T matrix elements in a least squares fit of the data.

Acknowledgements

This paper embodies the work of many accelerator physicists, primarily those who have worked upon the design of the SSC.

References

1. Conceptual Design of the Superconducting Super Collider. 1986. *SSC-SR-2020*, SSC Central Design Group, Berkeley, California
2. An Assessment of the Antiproton-Proton Option for the SSC. 1986. *SSC-SR-1022*
3. Heifets, S. 1986. *SSC-N-129*
4. Neuffer, D., Peggs, S. 1986. *SSC-63*
5. see for example Piwinski, A. 1986. *SSC-57*
6. Peggs, S. 1985. *Particle Accelerators,* 17 : pp. 11-50
7. Task Force on Commissioning and Operations. 1985. *SSC-SR-1005*
8. Aperture Task Force. 1985. *SSC-SR-1013*
9. Peggs, S. 1985. *SSC-N-45, 65, and 87*
10. Report of the Workshop on Realistic SSC Lattices. 1985. *SSC-SR-1015*
11. Peck, S. 1984. *Proc. of the 1984 Snowmass Workshop on the SSC,* p. 384. Fermilab, Batavia, Illinois
12. Peggs, S. 1985. *SSC-N-91*
13. Johnson, D. 1986. *SSC-N-151*
14. Dell, F. 1986. *SSC-N-132*
15. The Clustered Interaction Region Option for the SSC. 1985. *SSC-SR-1014*
16. Neuffer, D. 1984. *Appendix of SSC-2, submitted to Part. Acc.*
17. Tennyson, J. 1979. *AIP Conf. Proc. No. 57,* p. 158. AIP Press, New York
18. Evans, L. 1981. *CERN SPS/81-2,* CERN, Geneva
    Evans, L., Gareyte, J. 1982. *IEEE Trans. Nucl. Sci.,* NS-30 : 4
    Evans, L. 1983. *CERN SPS/83-38,* CERN, Geneva
19. Chirikov, B. 1979. *Phys. Reports,* 52 : 265
20. Peggs, S., Talman, R. 1986. *SSC-61*
21. Furman, M. 1986. *SSC-62*
22. Forest, E. 1986. *SSC-67*
23. Fisk, H. E. et al. 1985. *SSC-7*
24. Schachinger, L. 1986. *Unpublished*
25. Talman, R. 1986. *SSC-N-192*
26. Forest, E. 1986. Unpublished.
27. Peggs, S., Talman, R. 1986. Empirical Hamiltonians. *These Proceedings*
28. See for example Douglas, D., Dragt, A.1983. *Proc. 12th Int. Conf. on High Energy Accelerators,* Fermilab, Batavia, Illinois
29. Neuffer, D. 1986. *SSC-N-112*
30. Schachinger, L., Peggs, S. 1986. *SSC-N-149*
31. Schachinger, L., Talman, R. 1985. *SSC-52*
32. Peggs, S. 1983. *IEEE Trans. Nucl. Sci.,* NS-30 : 4
33. Talman, R. 1986. *Unpublished*
34. Edwards, D., Johnson, R., Willeke, F. 1985. *Fermilab-PUB-85/9,* Fermilab, Batavia, Illinois
35. Morton, P., et al. 1986. *Unpublished*
36. Peggs, S. 1986. *To be published in Proc. of the 1986 Snowmass Workshop on the SSC*